SANDIA REPORT
SAND2017-XXXX
Unlimited Release
Printed September 2017

Probability density of tunneled carrier states near heterojunctions calculated numerically by the scattering method

Samuel M. Myers, William R. Wampler and Normand A. Modine

Prepared by
Sandia National Laboratories
Albuquerque, New Mexico 87185 and Livermore, California 94550

Sandia National Laboratories is a multi-mission laboratory managed and operated by National Technology and Engineering Solutions of Sandia, LLC, a wholly owned subsidiary of Honeywell International, Inc., for the U.S. Department of Energy's National Nuclear Security Administration under contract DE-NA0003525.

Issued by Sandia National Laboratories, operated for the United States Department of Energy by National Technology and Engineering Solutions of Sandia, LLC.

Available to DOE and DOE contractors from
U.S. Department of Energy
Office of Scientific and Technical Information
P.O. Box 62
Oak Ridge, TN 37831

Telephone: (865) 576-8401
Facsimile: (865) 576-5728
E-Mail: reports@osti.gov
Online ordering: http://www.osti.gov/scitech

Available to the public from
U.S. Department of Commerce
National Technical Information Service
5301 Shawnee Rd
Alexandria, VA 22312

Telephone: (800) 553-6847
Facsimile: (703) 605-6900
E-Mail: orders@ntis.gov
Online order: http://www.ntis.gov/search

SAND2017-10494
Printed July 2017
Unlimited Release

Probability density of tunneled carrier states near heterojunctions calculated numerically by the scattering method

Samuel M. Myers and William R. Wampler
Radiation-Solid Interactions Department 1861
and
Normand A. Modine
Nanostructure Physics Department 1881

Sandia National Laboratories
P. O. Box 5800
Albuquerque, New Mexico 87185-MS1056

Abstract

The energy-dependent probability density of tunneled carrier states for arbitrarily specified longitudinal potential-energy profiles in planar bipolar devices is numerically computed using the scattering method. Results agree accurately with a previous treatment based on solution of the localized eigenvalue problem, where computation times are much greater. These developments enable quantitative treatment of tunneling-assisted recombination in irradiated heterojunction bipolar transistors, where band offsets may enhance the tunneling effect by orders of magnitude. The calculations also reveal the density of non-tunneled carrier states in spatially varying potentials, and thereby test the common approximation of uniform-bulk values for such densities.

TABLE OF CONTENTS

1. INTRODUCTION

Detrimental recombination of carriers at irradiation-defect traps in bipolar devices may be substantially increased by tunneling where the bands vary with location. This effect has been simulated by analytic treatments assuming a straight-line variation of the potential along the longitudinal device axis, as produced by a uniform internal field (See, e.g., Ref. 1). Recently one of us (Wampler) found that device models employing this approximation are inadequate for heterojunction bipolar transistors (HBTs), where composition-related band offsets approaching one-half electron volt may be superimposed on the field-induced slope. We previously developed a device model utilizing a numerical solution of the 1-D quantum-mechanical tunneling problem for an arbitrarily specified longitudinal potential, which yielded good consistency with experiments on Sandia devices [2, 3]. Additionally, an analytic approximation has been devised by Xujiao Gao in which the potential profile is represented by connected straight-line segments [4], pursuant to implementation in the Sandia codes CHARON [5] for devices and XYCE for circuits [6]. The device-relevant product of such calculations is the combined 3-D probability density of carrier states per unit energy E at the location x_t of a trap, $N_b(E,x_t)$. In simulations this quantity is combined with the E-dependent state-occupation probability and the E-dependent multiphonon reaction coefficient to obtain the carrier trapping rate [2,3].

In this report we describe a different numerical approach to the tunneling problem: impinging plane waves, with independently determined energy eigenvalues, are treated as scattered by the varying potential in the junction region to obtain the needed carrier probability densities. This contrasts with our previous use of an eigensolver to determine locally bounded wave functions [2,3]. The one-band envelope equation with the effective-mass approximation is employed in both cases, since higher-order two-band treatments [7] were previously found to be unnecessary for HBT modeling [3]. Computation time is reduced by orders of magnitude in the scattering method, but with reduced flexibility in configuring the problem, so that the approaches are complimentary. We compare results for $N_b(E,x_t)$ from the two methods and consider sensitivities to particulars of the calculations.

Our evaluation of state probability densities extends seamlessly into the non-tunneled regime where the energies of carriers are above that at the band edge. In addition to the direct

interaction with traps, this is where the processes of drift and diffusion occur. Modelers routinely assume bulk carrier properties in this regime. Our findings allow examination of the approximation.

2. METHOD

We deal first with the solution of the envelope equation to obtain carrier eigenstates, and then discuss their utilization to calculate the combined local density of states (DOS) $N_b(E,x_t)$. The 3-D one-band envelope equation for the planer heterojunction structure, and the associated wave functions and energy eigenvalues, are separable into axial components as

$$\Psi = \psi_x(x)\,\psi_y(y)\,\psi_z(z) \tag{1}$$

$$E = E_x + E_y + E_z \tag{2}$$

$$-\frac{\hbar^2}{2m}\frac{d^2}{dx^2}\psi_x(x) = \left[E_x - U(x)\right]\psi_x(x) \tag{3}$$

$$-\frac{\hbar^2}{2m}\frac{d^2}{dy^2}\psi_y(y) = E_y\psi_y(y) \tag{4}$$

$$-\frac{\hbar^2}{2m}\frac{d^2}{dz^2}\psi_z(z) = E_z\psi_z(z) \quad . \tag{5}$$

The Ψ and ψ are wave functions, the E are state energies, m is the effective mass of the carriers, and $\hbar$ is Planck's constant divided by 2π; U is the potential energy, corresponding to the band edge for conduction electrons and its negative for holes, which varies with location along the longitudinal x axis of the device. As in the previously discussed eigensolver approach [2, 3], Eqs. (4) and (5) are each treated analytically for an infinitively deep square well of width L much greater than the longitudinal dimension of the device. The resulting oscillatory solutions are real and non-degenerate with wave numbers and energy eigenvalues given by

$$K_{y,z}^{j} = \frac{1}{\hbar}\sqrt{2m\,E_{y,z}^{j}} = \frac{\pi}{L}j \quad \text{for positive integers } j \quad , \tag{6}$$

and average squared wave-function amplitudes 1/L corresponding to an integrated probability of 1.

The scattering approach is applied to an x-axis interval of varying potential U(x) bounded by two extended regions of respective constant potentials $U_{min} < U_{max}$, with the x-axis state energies being such that $U_{min} < E_x < U_{max}$. An idealized example that includes the principle features of a heterojunction structure is shown in Fig. 1, where a linear variation arising from a uniform internal field is interrupted by a step due to the abrupt composition change. Within the higher plateau on the left, the wave function is exponentially attenuated as x decreases, whereas in the plateau to the right the solution is oscillatory. The system is bounded on the right by an infinite step in U at the deeper end of the lower plateau.

A key property underlying the relative computational efficiency of the scattering approach is that, when the length of the lower-energy plateau is taken to be much larger than the range of varying potential, the energy eigenvalues E_x^j approach those for a square well given by

$$K_x^j = \frac{1}{\hbar}\sqrt{2m\left(E_x^j - U_{min}\right)} = \frac{\pi}{L}j \tag{7}$$

where L is the plateau dimension. With this independent knowledge of E_x^j it is not necessary to solve Eq. (3) as an eigenvalue problem requiring iteration; instead, the wave function for a given energy is obtained by a single numerical integration of the differential equation. The need to explicitly match phases between oscillations in the lower-plateau region and the more complex wave-function behavior near the junction is avoided by initiating the integration within the higher-energy plateau, where the dependence on x is a simple exponential. For convenience we equate the length of the lower x-axis plateau to the width of the square wells along the transverse axes. (Minute adjustment to achieve zero amplitude at the outer boundary is unnecessary for large L.)

The idealized x-axis potential profile used for the scattering calculations departs from physical reality with increasing distance from the tunneling region of interest. The assumed extent of the low-energy plateau exceeds by decades the actual width of structural features such as the base of HBTs, and also exceeds the scattering-limited coherence distance of the carriers, which may be in the nanometer range [3]. At the end of this section and in Sect. 3, we discuss

arguments and computational results supporting the insensitivity of pertinent carrier probability densities $N_b(E,x_t)$ to such idealizations at the periphery.

Discretizing the derivative in Eq. (3) yields a form suitable for numerical integration:

$$\psi_i^j = \left[2 - \frac{2m}{\hbar^2}\left(E_x^j - U_{i-1}\right)\left(\Delta x\right)^2 \right]\psi_{i-1}^j - \psi_{i-2}^j \quad \text{for } i \geq 3 \qquad (8)$$

where superscript j identifies the energy eigenvalue, subscript i is the position index for discretized x, and Δx is the corresponding increment. Subscripts denoting the x axis have been omitted from the discretized wave-function amplitudes for convenience. Pending normalization, ψ_1^j is equated to 1. Within the higher-energy plateau, where ψ_X increases exponentially with increasing x, one has [8]

$$\psi_2^j = \psi_1^j \exp\left(A\,\Delta x\right) \qquad (9)$$

where

$$A = \frac{1}{\hbar}\sqrt{2m\left(U_{max} - E^j\right)} \quad . \qquad (10)$$

After numerical integration to obtain the ψ_i^j, the wave functions are normalized so that the average squared amplitude over one oscillation in the lower-energy plateau is equal to 1/L, making the probability integrated over the entire interval L equal to 1. This numerical determination of the x-axis wave functions is computationally limiting, and is performed only for a single, representative eigenvalue E_x^j within each of the discretization intervals ΔE_X to be discussed.

The tunneled probability density at depth x_t for an individual 3-D eigenstate Ψ having total energy E and x-axis energy $E_X \leq E$ can be written

$$\left[\Psi(E,E_x,x_t)\right]^2 = \left[\left(\psi_x(E_x,x_t\right)\right]^2 \frac{1}{L^2} \qquad (11)$$

where the average squared amplitude 1/L is used for the y and z axial components of the wave function. Here, and in the following, it is sufficient and convenient to identify the eigenstates in

terms of continuum energies rather than indices because, at large L, any chosen value is negligibly distant from an actual eigenvalue. The combined energy-dependent probability DOS for tunneled carriers, $N_b(E,x_t)$, is obtained by summing the probability densities given by Eq. (11) for all states with total energies in a small interval from $E-\Delta E/2$ to $E+\Delta E/2$, and then dividing by ΔE. This summation is visualized as extending over one eighth of a spherical shell in the space of positive axial wave numbers $\{K_X,K_Y,K_Z\}$, wherein the coordinates of the eigenstates are uniformly distributed with axial spacing π/L, corresponding to a volume density of $(L/\pi)^3$. (Since the axial coordinates in wave-number space have units of reciprocal meters, the subject volume density is given as meters cubed. There are analogous inversions for area and distance.) The xy plane is depicted in Fig. 2, which shows a bounded element, with K-space area ΔA_K, that is determined by K, ΔK, K_X and ΔK_X where

$$K = \sqrt{K_x^{\,2} + K_y^{\,2} + K_z^{\,2}} \quad . \tag{12}$$

The corresponding ΔE and ΔE_X, related to ΔK and ΔK_X through Eqs. (6) and (7), are chosen to be invariant and equal. When the above planer element is projected a distance D_K along an arc about the x axis so as to traverse an angle of $\pi/2$, the number ΔS of contained eigenstate coordinates is given for small increments by

$$\begin{aligned} \Delta S &= \left(\frac{L}{\pi}\right)^3 D_K \Delta A_K \\ &= \left(\frac{L}{\pi}\right)^3 \left[\frac{\pi}{2}\left(K^2 - K_x^{\,2}\right)^{1/2}\right] \left[\frac{K\,\Delta K\,\Delta K_x}{\left(K^2 - K_x^{\,2}\right)^{1/2}}\right] \quad . \\ &= \frac{L^3}{2\pi^2} K\,\Delta K\,\Delta K_x \end{aligned} \tag{13}$$

A change of variables using Eqs. (6) and (7) gives

$$\Delta S = \frac{L^3}{2\pi^2\hbar^3} \frac{m^{3/2}}{\sqrt{2\left(E_x - U_{min}\right)}} \left(\Delta E\right)^2 \tag{14}$$

where the equality of ΔE and ΔE_x is assumed. Multiplying ΔS by the single-state probability density in Eq. (11), dividing by ΔE, and adding a factor of 2 for spin degeneracy gives the contribution $\Delta N_b(E,E_x,x_t)$ to the tunneled DOS $N_b(E,x_t)$ from the interval ΔE_x at x-axis energy $E_x \le E$:

$$\Delta N_b(E,E_x,x_t) = \frac{L}{\pi^2\hbar^3}\frac{m^{3/2}\Delta E}{\sqrt{2\left(E_x - U_{min}\right)}}\left[\left(\psi_x(E_x,x_t)\right)\right]^2 \quad . \tag{15}$$

As explained above, the normalization of the wave function is such that its squared amplitude is proportional to 1/L, so that ΔN_b is independent of L. It is therefore permissible to use L = 1 meter in the calculation.

In Refs. 2 and 3 we reported calculations of $N_b(E,x_t)$ in which the x-axis envelope equation, Eq. (3) above, was solved for locally bound potential wells having microscopic dimensions L_x comparable to or even smaller than the region of varying U(x) near the heterojunction. The fewer eigenstates, with energy eigenvalues not independently available, were obtained using an iterative eigensolver. This more computationally intensive method facilitates examination of the influences of model configuration and wave-function termination on the extracted DOS.

It is illuminating to compare the above Eq. (15) with the summation terms for $N_b(E,x_t)$ in the eigensolver approach, where each energy interval ΔE_x contains a single eigenvalue. Relative to Eq. (13) of Ref. 3, Eq. (15) has the additional factor

$$\frac{L}{\pi\hbar}\frac{m^{1/2}\Delta E_x}{\sqrt{2\left(E_x - U_{min}\right)}} \tag{16}$$

(except in the particular case of $E_x = E$ with $E_y = E_z = 0$). This expression can be shown to be the number of x-axis scattering eigenvalues E_x within the interval ΔE_x, which is consistent with the following physical insight. If the numerous x-axis scattering eigenstates within ΔE_x are replaced by a single state near the center of the interval, and if that state is artificially assigned a degeneracy equal to the actual number of states, then the summation of Ref. 3 should become applicable and yield results in accord with the present approach.

Pursuant to an optimal outcome from coarse energy discretization, we adopt a procedural detail from the earlier study [2,3]. In computing $N_b(E,x_t)$, the uppermost ΔE_x interval of the summation is centered on E, and the associated term is one-half of that given in Eq. (15). One then has

$$N_b(E,x_t) = \frac{1}{2}\Delta N_b(E,E_x = E,x_t) + \sum_{E_x<E} \Delta N_b(E,E_x,x_t) \quad . \tag{17}$$

In practice the lower limit of the summation is the higher of U_{min} or the energy of the trapped state.

The above scattering approach is based on the impingement of plane waves with independently known eigenvalues; as already noted, it implies an extended potential plateau not actually present in bipolar devices. When the plateau dimension L is large compared to the range of varying U(x), the number of states per unit energy and the amplitudes of the normalized wave functions near a given energy vary oppositely with L, compensating to produce an invariant probability density N_b as detailed above. These opposing dependences persist when L is comparable to the range of the varying potential, as can be shown using the WKB approximation of the wave function. In the following section and in Ref. 3, comparison of computational results between the scattering approach and the eigensolver method, combined with eigensolver calculations for multiple widths of the potential well, show good consistency indicative of accurate compensation for conditions of interest.

3. CALCULATIONS AND DISCUSSION

The scattering method discussed in Sect. 2 was applied to the problem represented in Fig. 1, with results shown in Fig. 3. The potential ramp corresponds to a field magnitude of 10 MV/m, typical of HBTs, while the step amplitude of 0.5 eV is near the upper end of values encountered in Sandia devices. The normalized effective mass m/m0 is 0.1, roughly representative of electrons and light holes in GaAs. The dimension of the three axial potential wells L is 1 meter. The numerical solution of Eq. (3) was carried to x = 500 nm, sufficient for characterization of the oscillatory wave function in the lower-energy plateau. Also shown is the result without the potential step, where the linear ramp is continued uninterrupted down to zero

potential. The large difference in the DOS illustrates the substantial influence of the band offset and the resultant need for a realistic description.

An equivalent problem was solved using the eigensolver approach of Refs. 2 and 3, with results included in Fig. 3. The potential profile in the localized well, with a width of 1000 nm rather than 1 meter, is shown in Fig. 4. The extent of the ramp is several times larger than in Fig. 1 in order to produce a suitable distribution of eigenstates, but relevant conditions near the step are identical. The execution time for the eigensolver calculation is about two orders of magnitude greater than for the scattering treatment, for reasons that were discussed in Sect. 2.

The consistency in Fig. 3 between the different methodologies and potential configurations is a favorable indication for the correctness of the results and their insensitivity to computational details. In this regard we also note a calculation reported in Refs. 2 and 3, where a potential well similar to that in Fig. 4 was narrowed to the point where the left wall intersected the ramp and was only 40 nm from the trap. While the energy separation of the x-axis eigenstates was greatly increased, sufficient resolution remained to demonstrate quantitative consistency of the tunneled DOS. This reflects the accurately compensating variations of wave-function normalization and number of states per unit energy that was discussed in Sect. 2.

As indicated above, our treatment of the energy-dependent probability density is believed to remain valid when the energies of the carrier states extend above that of the band edge at the location of the trap. While the local influence of tunneling ceases, the findings are pertinent to recombination by direct trapping, and also to the number of states contributing to transport by drift and diffusion. The bulk DOS is routinely considered to remain applicable in the regions of bipolar devices where the bands vary, and the accuracy of this approximation warrants examination. In Fig. 5 we show $N_b(E,x_t)$ in the non-tunneling regime under three conditions: the uniform bulk in zero field [9]; an extended potential ramp in a representative field of magnitude 10 MV/m; and, the same ramp interrupted by a 0.5 eV step located 0.05 eV down-slope from the trap. The small energy range of the plot is chosen to emphasize the region of significant thermal occupancy near room temperature. Inspection suggests modest errors in predicted device operating characteristics that can be offset through parameter calibration.

4. CONCLUSION

We have developed an efficient numerical method based on the scattering approach for calculating the combined probability density of tunneled carrier states in planer bipolar devices. This facilitates the description of band-to-trap tunneling under arbitrary longitudinal potential profiles, and is particularly useful in modeling carrier recombination in irradiated heterojunction bipolar transistors. The approach is also applicable to non-tunneled carriers, and could be used to refine descriptions of direct carrier reactions and transport via drift-diffusion.

In present form our calculation treats carriers impinging from a single direction, and employs the one-band envelop equation with the effective-mass approximation. We have found these simplifications to be acceptable in modeling HBTs. The scattering approach can accommodate incidence from two directions, including circumstances where the carrier chemical potentials on the two sides are different, but such a calculation is substantially more complicated. Also feasible is implementation of the two-band Flietner model [10], which is expected to describe tunneling far from the band edge more realistically than the effective-mass approximation.

ACKNOWLEDGMENTS

We benefited from discussions with Xujiao (Suzey) Gao concerning carrier tunneling.
Sandia National Laboratories is a multi-mission laboratory managed and operated by National Technology and Engineering Solutions of Sandia, LLC, a wholly owned subsidiary of Honeywell International, Inc., for the U.S. Department of Energy's National Nuclear Security Administration under contract DE-NA0003525

REFERENCES

1. A. Schenk, Solid-State Electron. **35**, 1585 (1992).
2. S. M. Myers, W. R. Wampler, and N. A. Modine, *Recombination by band-to-defect tunneling near heterojunctions in irradiated bipolar devices: a theoretical model*, Sandia Report, SAND2015-7650, September 2015
3. S. M. Myers, W. R. Wampler, and N. A. Modine, J. Appl. Phys. **120**, 134502 (2016).
4. X. Gao, private communication, 2017.
5. G.L. Hennigan, R.J. Hoekstra, J.P. Castro, D.A. Fixel and J.N. Shadid, *Simulation of Neutron Radiation Damage in Silicon Semiconductor Devices*, Sandia Report, SAND2007-7157, October 2007
6. E.R. Keiter, K.V. Aadithya et al, *Xyce Parallel Electronic Simulator Users' Guide Version 6.7*, Sandia Report, SAND2017-4931, May 2017
7. A. Pan and C. O. Chui, J. Appl. Phys. **116**, 054508 & 054509 (2014); H. Carrillo-Nuñez, A. Ziegler, M. Luisier, and A. Schenk, J. Appl. Phys. **117**, 234501 (2015); and references therein.
8. E. Merzbacher, Quantum Mechanics (Wiley, 1961), p. 87.
9. S. M. Sze and K. K. Ng, Physics of Semiconductor Devices (Wiley, 2007), p. 17.
10. H. Flietner, Phys. Stat. Sol. B **54**, 201 (1972).

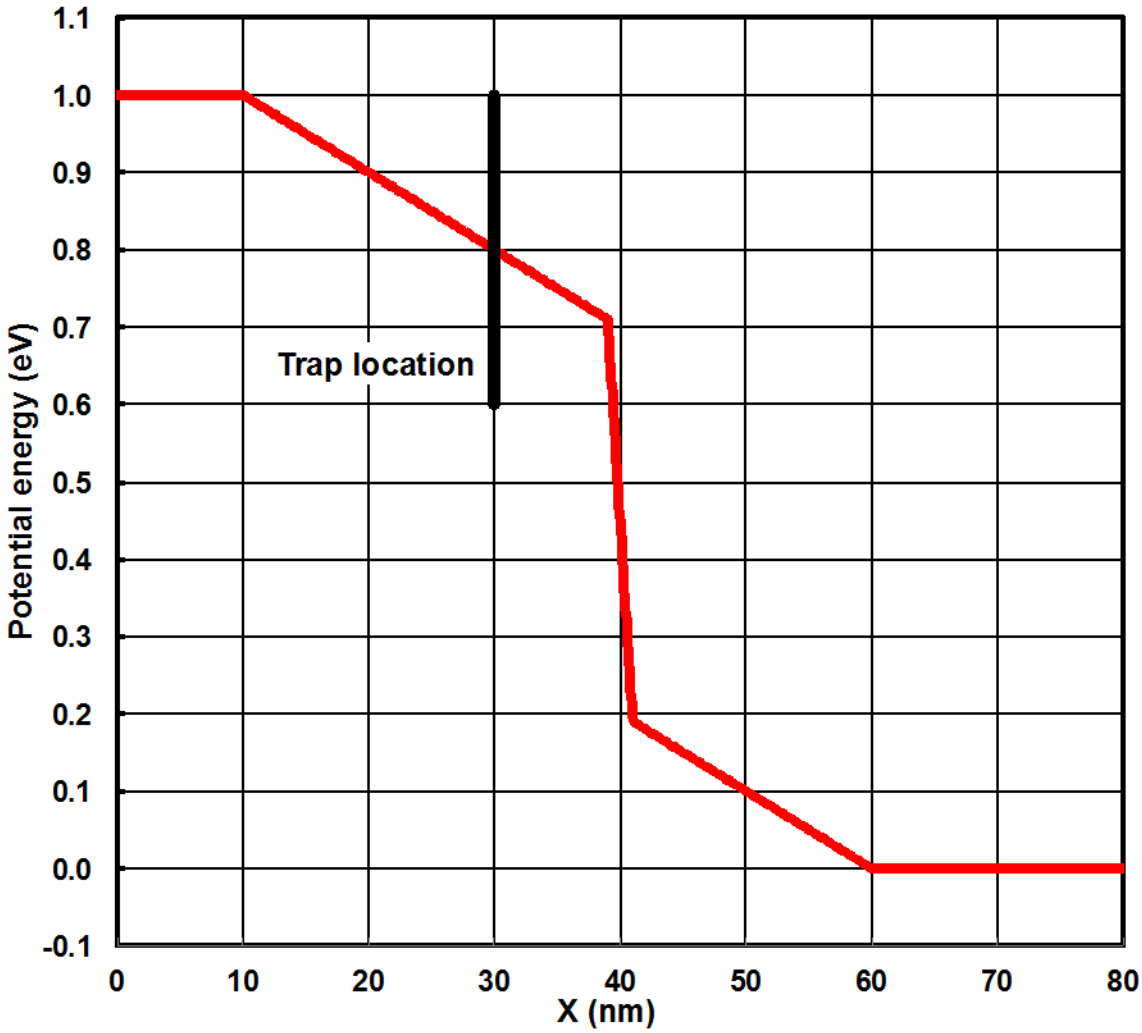

Figure 1. Profile of carrier potential energy U versus depth x for an idealized heterojunction having a uniform internal field of magnitude 10 MV/m and a band offset of 0.5 eV, which is used to calculate the tunneled probability density of states at a trap by the scattering approach. The trap is located at 30 nm, with tunneling occurring from the band region on the right.

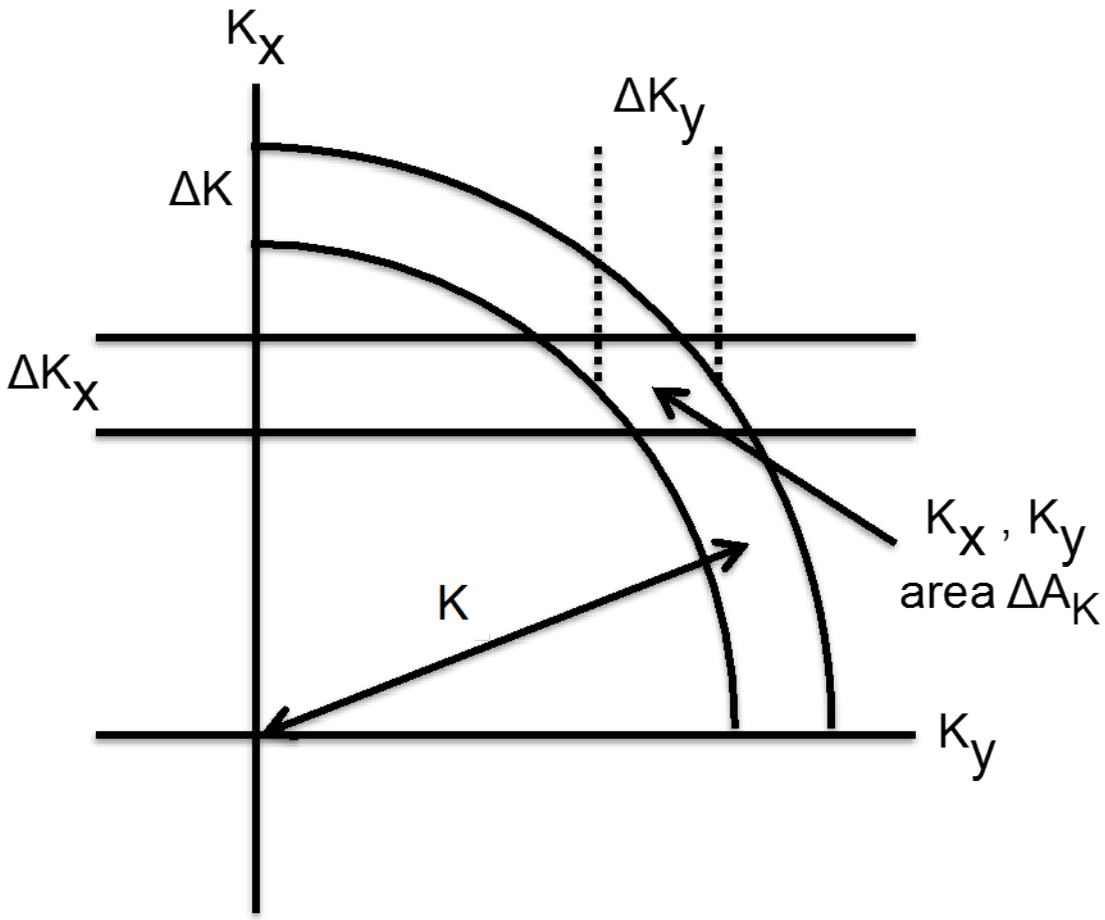

Figure 2. Diagram of the xy plane in $\{K_x,K_y,K_z\}$ space used to formulate the summation over carrier eigenstates. All coordinates within each x-axis interval ΔK_x connect to a single numerical evaluation of $\psi_x(E_x,x_t)$.

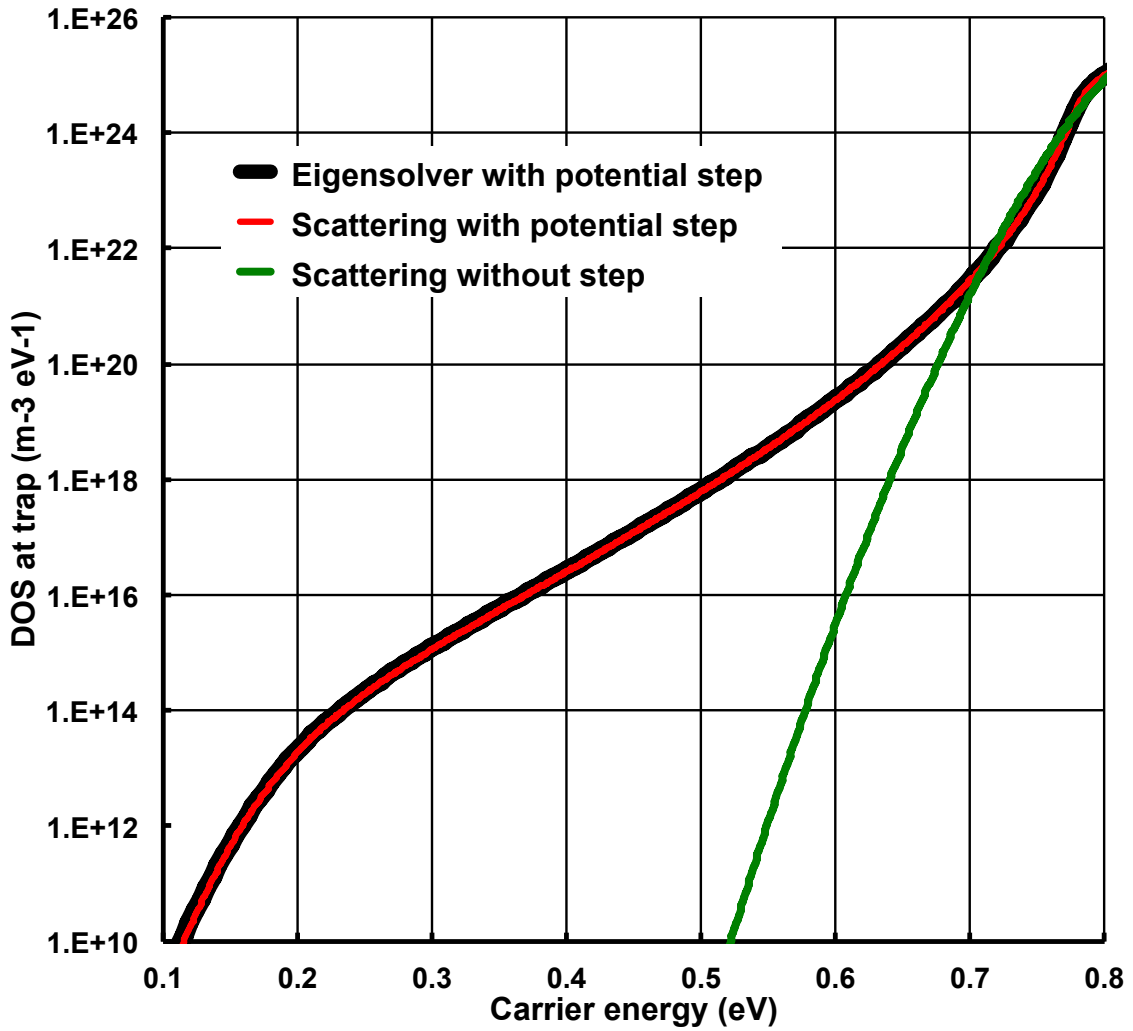

Figure 3. Tunneled probability densities of carrier states at the trap, $N_b(E,x_t)$, obtained by the scattering approach for the conditions of Fig. 1 with and without the potential-energy step. The band edge at the location of the trap is at 0.8 eV, corresponding to the right margin. A corresponding result from the eigensolver method is included for comparison. These results illustrate the large influence of the band offset.

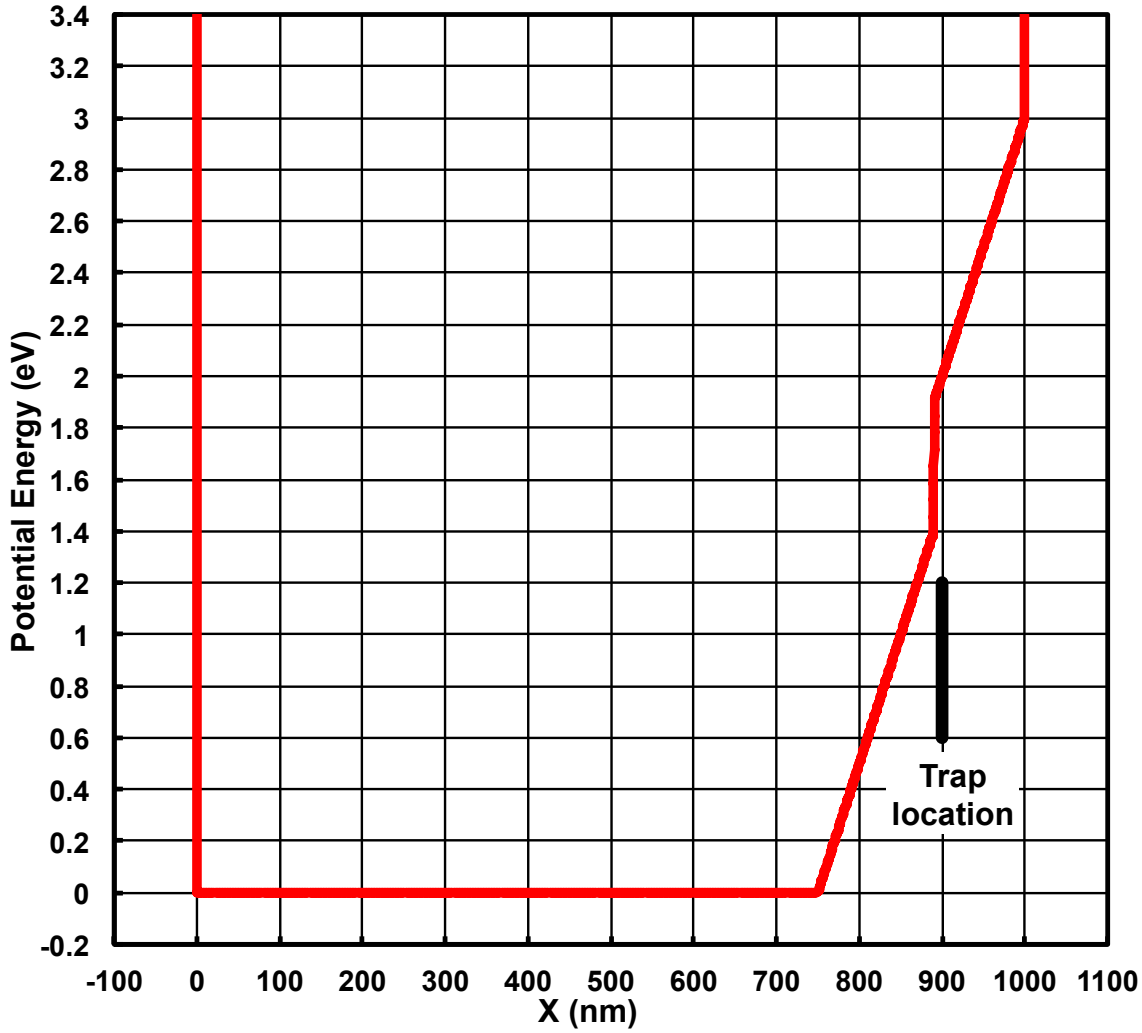

Figure 4. Potential-energy profile used to calculate the tunneled density of states in Fig. 3 by the eigensolver method. The potential well dimension of 1000 nm, and the elongated ramp below the step, are chosen to produce a suitable distribution of eigenstates and x-axis discretization. The region of interest near the step is equivalent to that in Fig. 1.

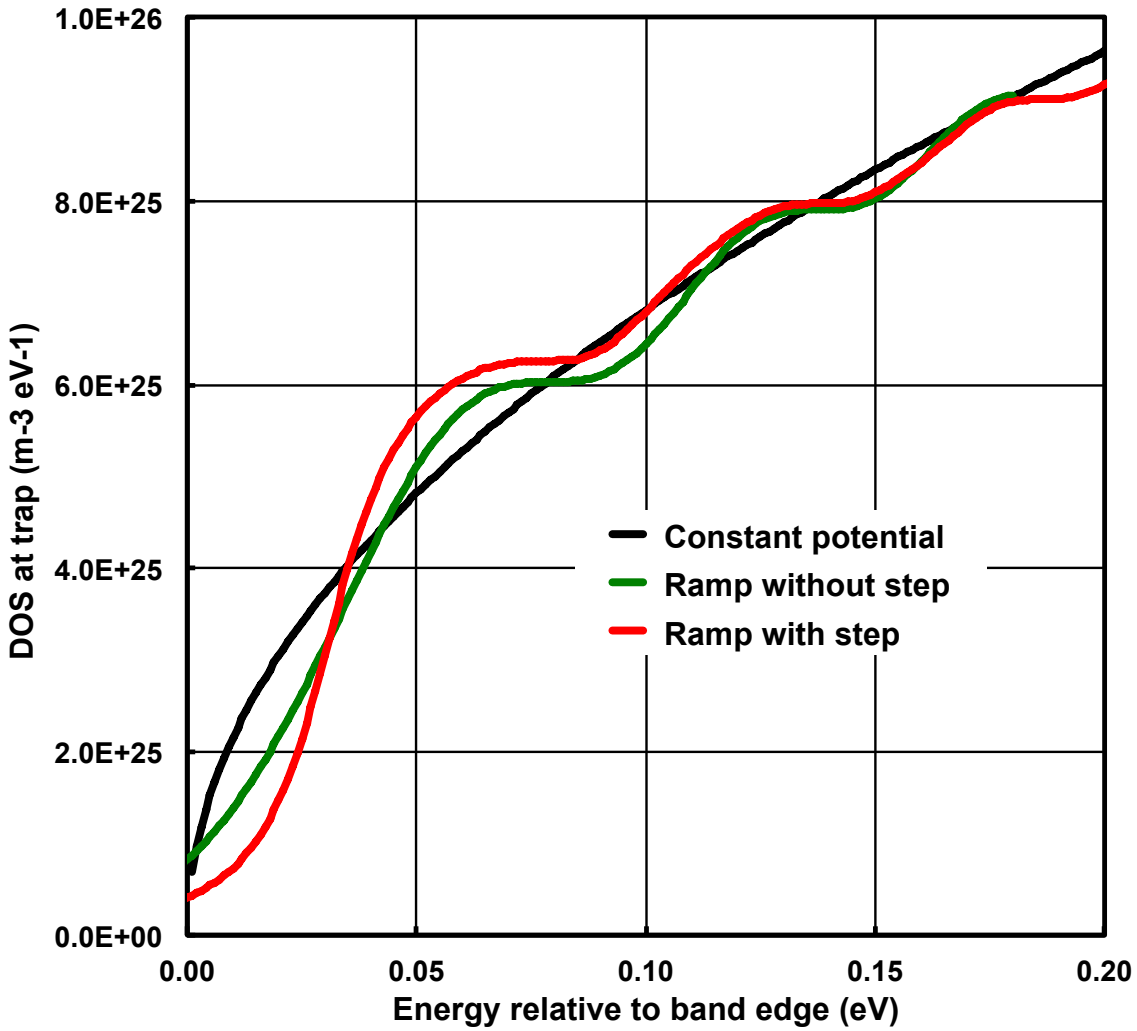

Figure 5. Densities of states at energies above the band edge for a constant potential; for a ramp corresponding to a field magnitude of 10 MV/m; and for a ramp with a 0.5 eV step located 0.05 eV down the ramp from the trap.

DISTRIBUTION

1	MS0899	Technical Library	9536 (electronic copy)
1	MS1179	Leonard Lorence	1341 (electronic copy)
1	MS1177	Xujiao Gao	1355 (electronic copy)
1	MS1177	Gary Hennigan	1355 (electronic copy)
1	MS1177	Eric Keiter	1355 (electronic copy)
1	MS1177	Joseph Castro	1355 (electronic copy)
1	MS1315	Normand Modine	1881 (electronic copy)


Sandia National Laboratories